Matter

CellPress

Article

Fabricating hydrogels to mimic biological tissues of complex shapes and high fatigue resistance

Hang Yang,[1,2,4] Mengke Ji,[1,4] Meng Yang,[1] Meixuanzi Shi,[1,2] Yudong Pan,[1] Yifan Zhou,[1] Hang Jerry Qi,[3] Zhigang Suo,[2,*] and Jingda Tang[1,5,*]

SUMMARY

Biological tissues, such as heart valves and vocal cords, function through complex shapes and high fatigue resistance. Achieving both attributes with synthetic materials is hitherto an unmet challenge. Here we meet this challenge with hydrogels of heterogeneous structures. We fabricate a three-dimensional hydrogel skeleton by stereolithography and a hydrogel matrix by cast. Both the skeleton and matrix are elastic and stretchable, but the skeleton is much stiffer than the matrix, and their polymer networks entangle topologically. When such a hydrogel is stretched, the compliance of the matrix deconcentrates stress in the skeleton and amplifies fatigue resistance. We fabricate a homogeneous hydrogel and a heterogeneous hydrogel, each in the shape of a human heart valve. Subject to cyclic pressure, the former fractures in ~560 cycles but the latter is intact after 50,000 cycles. Soft materials of complex shapes and high fatigue resistance open broad opportunities for applications.

INTRODUCTION

Soft biological tissues typically consist of large amounts of water (30–80 wt %) and networks of flexible polymers.[1] The water molecules provide a liquid medium in which other molecules migrate and react. The polymer networks enable solid properties such as elasticity, toughness, and fatigue resistance.[2,3] These tissues often have complex shapes and heterogeneous structures. For instance, a heart valve has the shape needed to regulate blood flow and consists of an extracellular matrix and multiple layers of collagen fiber bundles (Figure 1A).[4,5] A healthy human heart valve beats ~3 billion times in a lifetime.[6]

Soft biological tissues have been mimicked using synthetic hydrogels.[2,7–9] Applications include tissue repair,[10] regenerative medicine,[1] and soft robots.[11] Evidence has accumulated recently that synthetic hydrogels, unlike biological tissues, are susceptible to fatigue fracture.[3] It is likely that biological tissues achieve fatigue resistance through heterogeneous structures with strong adhesion between materials.[12] Transformative advances have been made recently on strong hydrogel adhesion.[13] The basic principle relies on the synergy of interfacial bonds, topology of polymer networks, and mechanical dissipation of the adherends. The reported approaches include surface modification,[14] bulk modification,[15] diluted cyanoacrylate,[16] bridging polymers,[17] and topological adhesion.[18] In addition, various reinforced hydrogel composites have been fabricated to mimic the microstructure of natural tissues.[19] Stiff fibers (e.g., glass fibers, plastic fibers) have been embedded into

Progress and potential

A long-standing hurdle is to synthesize hydrogels of complex shapes and high fatigue resistance. These attributes are prerequisites for the functions of many biological tissues, such as heart valves and vocal cords. This paper demonstrates that complex shapes and high fatigue resistance can be achieved with hydrogels of heterogeneous structures. Using a combination of stereolithography and cast, we fabricate a heterogeneous hydrogel consisting of a skeleton and a matrix, and their polymer networks entangle topologically. The heterogeneous hydrogel achieves a fatigue threshold of ~400 J/m^2, a remarkable value considering the fatigue threshold of natural rubber is ~50 J/m^2. We fabricate a homogeneous hydrogel and a heterogeneous hydrogel, each in the shape of a human heart valve. The homogeneous hydrogel fractures after ~560 cycles but the heterogeneous hydrogel remains intact after 50,000 cycles.

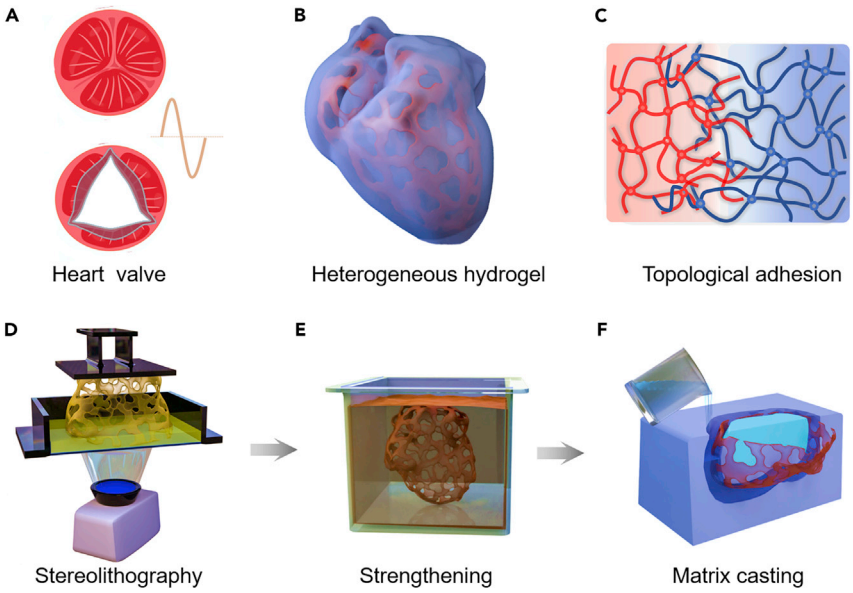

Figure 1. Heterogeneous structure of complex shape

(A) A biological tissue, such as a heart valve, functions through a complex shape and high fatigue resistance. The tissue has a heterogeneous structure.

(B) A hydrogel is made in the shape of a heart, consisting of a skeleton and a matrix of large modulus contrast.

(C) The polymer networks of the skeleton and matrix entangle topologically.

(D–F) Fabrication process of the heterogeneous hydrogels with complex shape and high fatigue resistance.

hydrogels to enhance the modulus and toughness,[20–22] while stiff fibers will constrain the stretchability. Very recently, soft fibers reinforced composite have been proposed to increase the toughness and fatigue resistance of soft materials as well as maintain the high stretchability.[23,24] Elastomer fibers have been embedded into hydrogels to achieve a fatigue threshold above 1,000 J/m^2.[25] The materials reported so far, however, have simple shapes such as sheets, blocks, and cylinders.

Here, we realize complex shapes and high fatigue resistance with hydrogels of heterogeneous structures. Such a hydrogel consists of a skeleton and a matrix (Figure 1B). Both constitutes are elastic and stretchable, but the skeleton is much stiffer than the matrix. Their polymer networks entangle topologically—that is, the entanglement is invariant when the hydrogel deforms unless at least one network breaks (Figure 1C). A fatigue threshold of ~400 J/m^2 is achieved. This value is remarkable considering that the fatigue threshold of natural rubber is ~50 J/m^2.[26] We fabricate a heterogeneous hydrogel and a homogeneous hydrogel, both in the shape of a human heart valve. The heterogeneous hydrogel remains intact after 50,000 cycles, whereas the homogeneous hydrogel fractures after ~560 cycles.

RESULTS AND DISCUSSION

Fabrication of the heterogeneous hydrogel

The object of this paper is to demonstrate that hydrogels can achieve both complex shapes and high fatigue resistance. We do so by fabricating a heterogeneous structure with a particular set of processes and materials (Figures 1D-F and S1). To achieve high fatigue resistance, the two constituent hydrogels should have

[1]State Key Laboratory for Strength and Vibration of Mechanical Structures, International Center for Applied Mechanics, Department of Engineering Mechanics, Xi'an Jiaotong University, Xi'an 710049, China

[2]John A. Paulson School of Engineering and Applied Science, Kavli Institute for Bionano Science and Technology, Harvard University, Cambridge, MA 02138, USA

[3]The George W. Woodruff School of Mechanical Engineering, Georgia Institute of Technology, Atlanta, GA 30332, USA

[4]These authors contributed equally

[5]Lead contact

*Correspondence: suo@seas.harvard.edu (Z.S.), tangjd@mail.xjtu.edu.cn (J.T.)

https://doi.org/10.1016/j.matt.2021.03.011

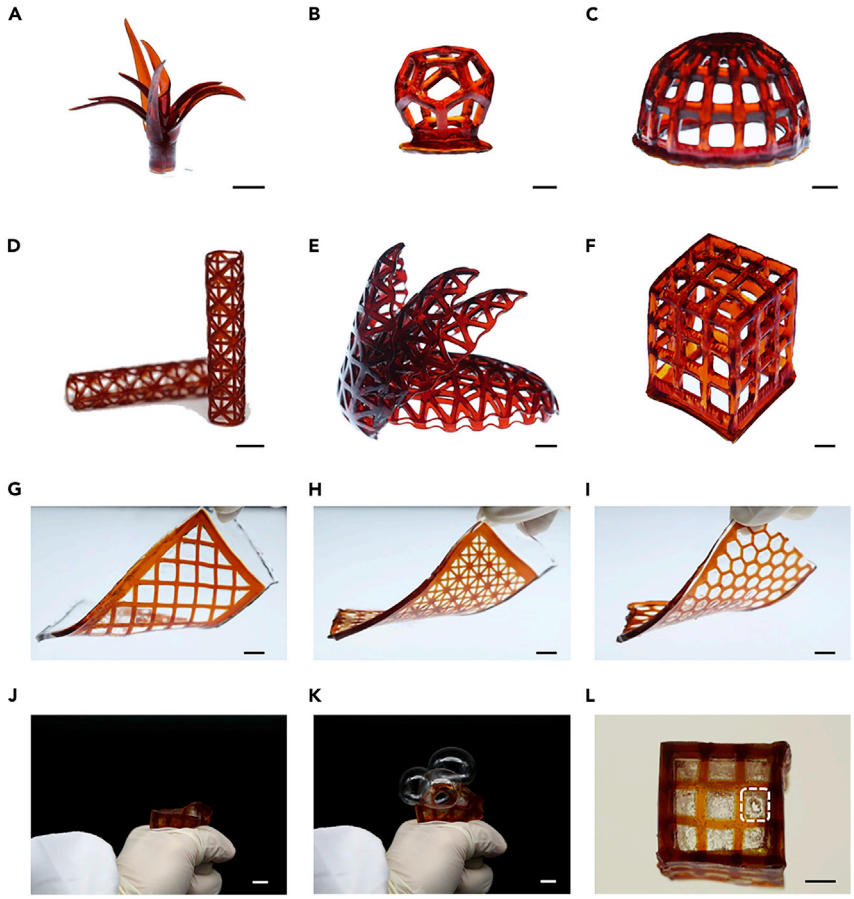

Figure 2. Skeletons and skeleton-matrix composites

(A–F) Skeletons of various shapes fabricated with stereolithography. (A) Orchid-like structure. (B) Hollow sphere composed of pentagons. (C) Hollow hemisphere. (D) Hollow tube. (E) Hollow shell structure. (F) Hollow cube with an open face.

(G–I) Heterogeneous hydrogels with two-dimensional skeletons. (G) Diamond pattern. (H) Square with cross lines. (I) Hexagon pattern.

(J–L) When a composite cube is inflated by air, it bulges slightly (J), balloons suddenly (K), and ruptures at a random location (L). The crack is restricted inside a unit square by stiff fibers (marked by white dashed lines).

Scale bars, 1 cm.

large modulus contrast and strong adhesion at the interface. We choose polyacrylamide-polyacrylic acid (PAAm-PAA) hydrogel strengthened by the carboxyl-Fe^{3+} complexes as the skeleton because of its high modulus of ~1 MPa. We choose PAAm hydrogels as the soft matrix because of its low modulus of 0.01–0.1 MPa. The precursor for the skeleton consists of acrylamide (AAm) and acrylic acid (AA) as monomers, *N*,*N*′-methylenebis-(acrylamide) (MBAA) as the crosslinker, 2,4,6-trimethyl benzoyl-diphenylphosphine oxide (TPO) nanoparticle as the initiator,[27,28] and tartrazine as a dye.[29] The ingredients are dissolved in water and then exposed to UV light. An initiator induces a free radical on a monomer, and the two types of monomers copolymerize into PAAm-PAA chains. Each AA monomer contributes a carboxyl group COO^-. We immerse the PAAm-PAA hydrogel in an aqueous solution of $FeCl_3$ to form carboxyl-Fe^{3+} complexes between polymer chains.[30,31] The skeleton is further immersed in deionized (DI) water to remove extra ions.

We make a hydrogel skeleton of various shapes (Figures 2A–2F) by stereolithography.[29,32] We fit a skeleton in a mold, inject the PAAm precursor into the mold, and polymerize a hydrogel matrix. Because the precursor of the matrix readily migrates into the polymer network of the skeleton, the polymer networks of the matrix and skeleton entangle topologically (Figure 1C). We cast the matrix around two-dimensional (2D) skeletons (Figures 2G, 2H, 2I, and S2) and cast a thin layer of matrix on a skeleton of a hollow cube with an open face (Figure 2F).

To demonstrate that the heterogeneous hydrogel is airtight, we inflate the cube with air (Video S1). As the pressure increases, the cube bulges slightly, balloons suddenly, and ruptures at a random location (Figures 2J, 2K, and 2L). The crack is restricted by the skeleton inside a unit square (marked by dashed white lines in Figure 2L).

Stereolithography can make structures of small feature sizes. The printed hydrogel shows a feature size <100 μm (Figure S3). The straight lines in Figure S3A have a width ranging from 92 to 410 μm. The resolution of the print is affected by the composition of the precursor (Figure S3B). We fix the printed model as a straight line of a prescribed width of 1,000 μm and measure the width of the prints at an exposure time of 240 s. The width of the print decreases as the concentration of the photoinitiator (PI) decreases and the concentration of the dye increases. The resolution of the prints can be further enhanced by employing a projector of a higher resolution,[33] but this is not pursued here.

The above strategy of fabricating heterogeneous hydrogel is universal to various material species. We have prepared heterogeneous hydrogels with different soft hydrogel matrices such as poly(*N*-isopropyl acrylamide) (PNIPAm), poly(hydroxyethyl methacrylate) (PHEMA), and gelatin (Figure S4). We also print different stiff hydrogel skeletons using a PAAm/alginate system strengthened by various ions, such as ferric ion (Fe^{3+}), aluminum ion (Al^{3+}), copper ion (Cu^{2+}), and barium ion (Ba^{2+})[34] (Figure S5). These alternative material systems provide us with a myriad of choices for preparing heterogeneous hydrogel.

Mechanical design and properties

We separately measured the properties of the two constituents. The ultimate stretch is ~20 for the soft hydrogel and ~4 for the stiff hydrogel (Figure 3A). The soft hydrogel has a modulus of 0.042 MPa, and all the stiff hydrogels have a high modulus of ~1 MPa (Figure 3B). The complex-crosslinked hydrogel has a large properties space. A long immersion time and a large weight ratio of AA to AAm will yield a high modulus (Figure S6).

The polymer networks of the soft hydrogel and stiff hydrogel entangle topologically. We observed the diffusion of the precursor of the soft hydrogel into the stiff hydrogel in a confocal microscope (Figure 3C). The diffusion length of the precursor increases with time and reaches a depth on the order of 100 μm. Considering that the mesh size of the polymer network of the hydrogel is on the order of 10 nm,[35] this large diffusion length guarantees topological entanglement between the two constituent hydrogels. We conducted a peel test and record the force as a function of the displacement (Figure S7). The adhesion energy is comparable with the bulk toughness of the soft hydrogel (185 ± 41 J/m^2) (Figure 3F).

We measured the toughness of a heterogeneous hydrogel (Figure 3D). We prepared a rectangular sheet of a stiff hydrogel with circular holes and then cast a soft hydrogel throughout the sheet. The sheet is gripped at the top and bottom with two rigid

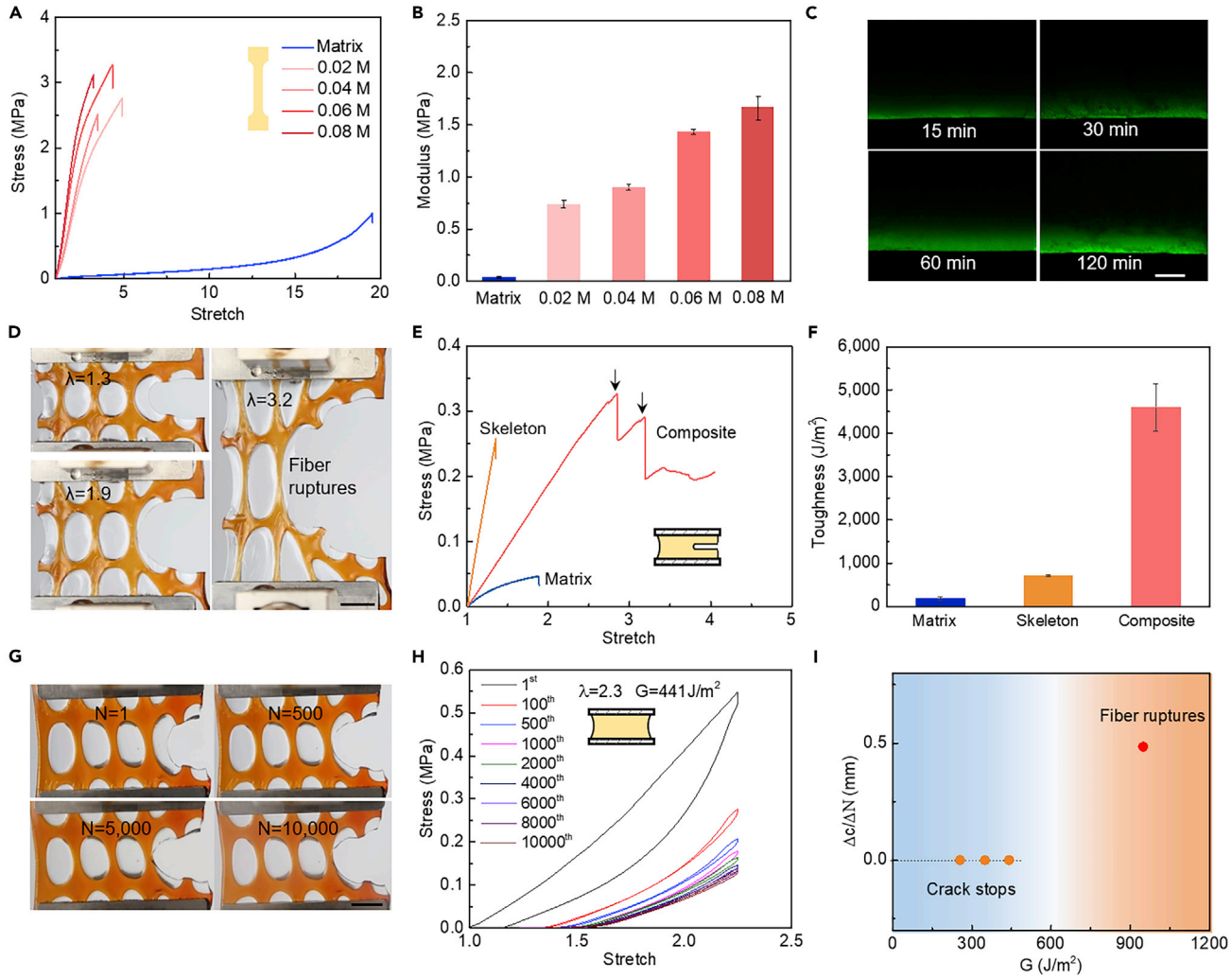

Figure 3. Mechanical properties

(A) The stress-stretch curves of the soft hydrogel and the stiff hydrogels are immersed in ferric solutions with various Fe^{3+} concentrations.

(B) Moduli of soft matrix and stiff hydrogels.

(C) Confocal images show the diffusion of the precursor of the soft hydrogel into the stiff hydrogel. Scale bar, 200 μm.

(D) Fracture images of the heterogeneous hydrogel. Scale bar, 1 cm.

(E) Stress-stretch curves of notched samples for the matrix (PAAm hydrogel), skeleton (strengthened PAAm-PAAhydrogel), and composite hydrogel.

(F) Comparison of the toughness between homogeneous and composite hydrogel.

(G) The composite hydrogel is fatigue resistant. Scale bar, 1 cm.

(H) Stress decline for a sample without precut crack under cyclic stretch.

(I) Fatigue behavior of the composite hydrogel at different energy release rates.

clamps and is cut with a crack using a razor blade. When the clamps are pulled relative to each other, the crack blunts before it propagates. The compliance of the soft hydrogel deconcentrates stress in the stiff hydrogel—that is, before a ligament of the stiff hydrogel ruptures, the entire ligament is stretched. When the ligament ruptures, the energy stored in the entire ligament is dissipated. This stress deconcentration leads to high toughness. We also fabricated rectangular sheets of homogeneous soft hydrogels and stiff hydrogels and conducted the same fracture test. The heterogeneous hydrogel ruptures at a larger stretch than the two constituent hydrogels (Figure 3E). The saw-toothed curve of the heterogeneous hydrogel corresponds to the rupture of successive ligaments. The experimental data enabled us

to determine the toughness of the three hydrogels (Figure S8A). The toughness of the heterogeneous hydrogel is 4,599 $\pm$ 545 J/m^2, much higher than that of the stiff hydrogel (710 $\pm$ 19 J/m^2) and the soft hydrogel (186 $\pm$ 41 J/m^2) (Figure 3F). The heterogeneous hydrogel shows a modulus of~0.18 MPa, between that of the stiff fiber and the soft matrix (Figure S8B). We also fabricate 2D sheets containing hollows of different shapes, such as triangles and hexagons (Figure S9). These heterogeneous hydrogels are also stretchable and tough.

We characterized the fatigue of the heterogeneous hydrogel by cyclically displacing the two rigid clamps relative to each other.[36] A sample is precut with a crack and stretched from $\lambda = 1$ to $\lambda_{applied}$ repeatedly at a frequency of ~0.2 Hz. For example, when $\lambda_{applied} = 2.3$, the crack does not propagate after 10,000 cycles (Figure 3G). We also cyclically stretched samples without a precut crack (Figure 3H). The maximum stress drops continuously and reaches a steady state at around 8,000 cycles. The stress-stretch curve at 10,000th cycle is used to calculate the energy release rate G.[3] The stress decay and the experimental photos are shown in Figure S10. We summarize the results in Figure 3I: the heterogeneous hydrogels fail through ligament rupture when $G > 948$ J/m^2, but the fatigue crack does not propagate when $G < 441$ J/m^2. This value is taken to be an estimate of the fatigue threshold.

In Figure S11we summarize the fatigue resistance versus modulus in the Ashby plot to compare the heterogeneous hydrogel in this paper with various hydrogels and biological tissues. The fracture energy of the human knee joint is above 1,000 J/m^2 after prolonged cycles.[37,38] The porcine bioprosthetic heart valve can maintain part of its flexural rigidity after 1 million cycles.[39] It is seen that the fatigue threshold of the heterogeneous hydrogel is comparable with biological tissues.

Adhesion between the constituents is vital for achieving high fatigue resistance. For a heterogeneous hydrogel with weak adhesion, the crack grows in the matrix even though the skeleton remains intact (Figure S12).

Heterogeneous hydrogel fabricated valve

We fabricated a homogeneous hydrogel and a heterogeneous hydrogel, each in the shape of a human heart valve. The clinical image data of a tricuspid valve was used to establish a computer-aided design (CAD) model (Figure 4A). The CAD model was converted into a printable digital model for printing a homogeneous hydrogel structure (Figure 4B). To fabricate a heterogeneous hydrogel, we modified the CAD model into a hollow one (Figure 4C). The as-printed hollow structure was immersed in the $FeCl_3$ solution, and a matrix was then cast to form a heterogeneous hydrogel (Figure 4D). In the heterogeneous hydrogel the skeleton provides the stiffness needed to regulate flow, and the matrix is soft enough to deconcentrate stress in the skeleton but stiff enough to sustain the pressure of the flow.

To evaluate the fatigue resistance of the two hydrogels, we designed an *in vitro* testing system (Figure 4E). The hemodynamic test system consists of a pump, a manometer, an endoscope, and a gripping flange (Figure S13). In the fatigue test, the homogeneous hydrogel fails around the margin after 560 cycles, while the heterogeneous hydrogel is intact even after 10,000 cycles (Figure 4F) (Videos S2 and S3). Figure 4G shows the fluctuation of the pressure drop ΔP across the hydrogel versus the cycle number. For the homogeneous hydrogel, the pressure drop ΔP decreases abruptly when it fails due to the free flow of the fluid, whereas the pressure drop for the heterogeneous hydrogel remains constant during 50,000 cycles.

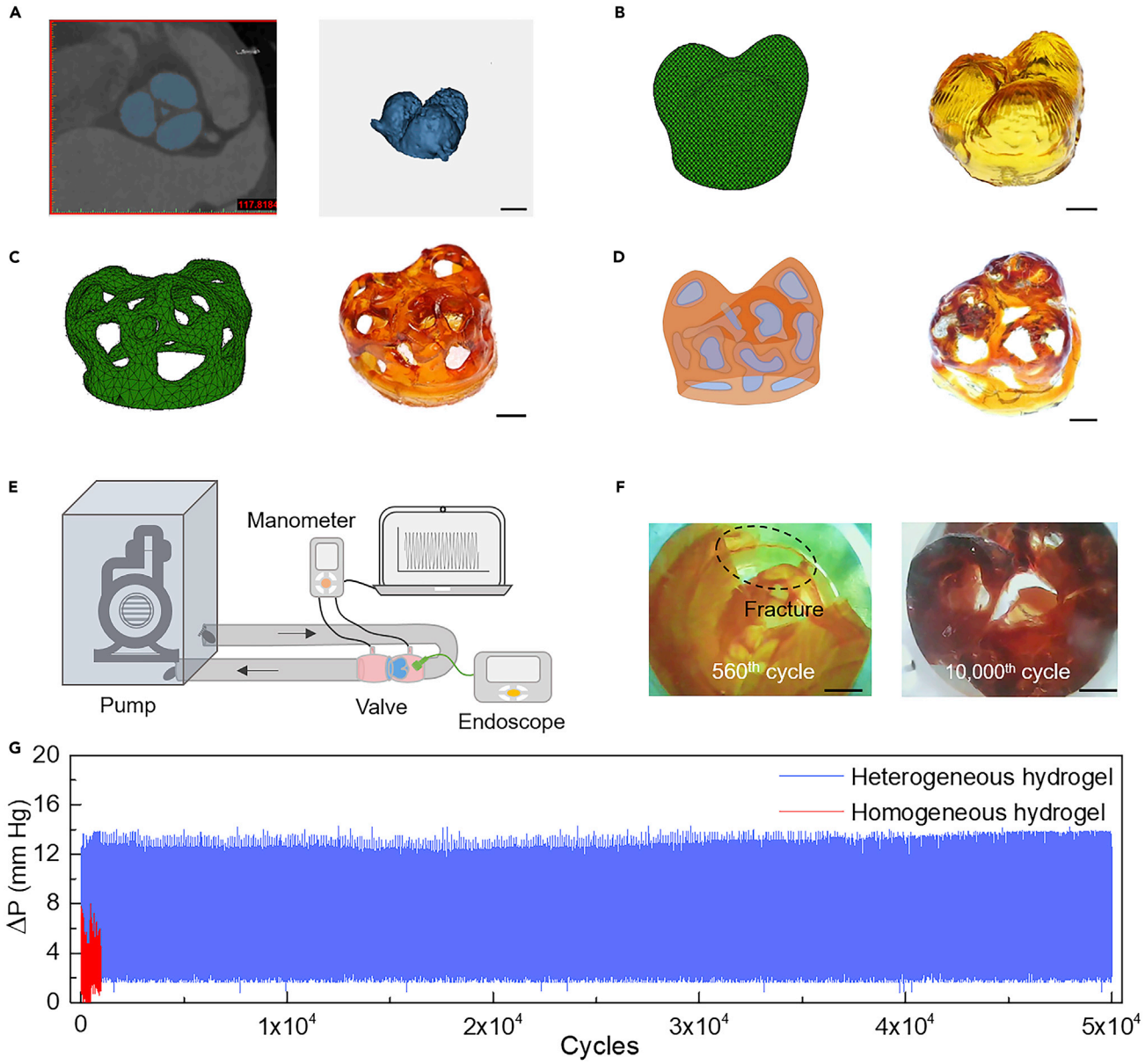

Figure 4. Hydrogel structures fabricated using the medical images of heart valves

(A) Computed tomography image and a computational model of a heart valve.

(B) Digital model and photo of the printed homogeneous hydrogel.

(C) To fabricate a heterogeneous hydrogel structure, a hollow model is established. The printed hollow hydrogel is further strengthened to form a stiff hydrogel skeleton.

(D) Schematic and photo of the heterogeneous hydrogel.

(E) Schematic of the setup to carry out the *in vitro* fatigue test.

(F) Endoscopic images of the homogeneous and heterogeneous hydrogels. The homogeneous structure fails at the margin after ~560 cycles, but the heterogeneous one stays intact even after 10,000 cycles.

(G) Fluctuation of the pressure drop ΔP across the structures with cycles.

Scale bars, 1 cm.

To evaluate the stress distribution of the hydrogel heart valve, we conducted simulation with commercial software (COMSOL Multiphysics®). The stress map is shown in Figure S14. It is seen that the maximum stress occurs at the root of the leaflet, which coincides with the rupture location of the valve in Figure 4F.

Conclusions

The combination of stereolithography and cast is convenient for open shapes such as heart valves but does not apply to closed shapes such as spherical shells. This approach can be used to fabricate complex shapes for other types of hydrogels, such as double network hydrogels[40] and microgel-reinforced hydrogels.[41] A hydrogel such as polyvinyl alcohol can self-assemble structures at microscale and nanoscale and achieve high fatigue resistance.[42] Complex shapes of such a hydrogel may be fabricated by stereolithography without the step of casting a matrix. Also, note that the additive manufacturing of hydrogels is in a state of flux.[5,27,29,43,32,44] Developing alternative heart valve has remained challenging over decades because of the highly demanding mechanical and biological requirements of real heart valves.[45] The demonstrated heterogeneous hydrogel probably cannot meet all these requirements and may not be satisfying for the *in vivo* microenvironments. The real heart valve shows negligible hysteresis in the loading-unloading cycles[46] while the composite hydrogel shows stress decay under cyclic load. The stress decay results from the breaking of carboxyl-Fe^{3+} coordination bonds in the PAAm-PAA hydrogel.[47] A stiff hydrogel with low hysteresis and high modulus is desired to better mimic the heart valve. It is not our intention here to work through many processes and materials. Rather, we demonstrate that complex shapes and high fatigue resistance can be achieved with hydrogels of heterogeneous structures. This central idea overcomes a long-standing hurdle and opens immediate and significant possibilities. It is hoped that work will soon follow to create synthetic heart valves that fulfill the mechanical function as well as biocompatibility.

EXPERIMENTAL PROCEDURES

Resource availability

Lead contact

Further information and requests for resources and reagents should be directed to and will be fulfilled by the lead contact, Jingda Tang (tangjd@mail.xjtu.edu.cn).

Materials availability

The materials generated in this study are available from the corresponding author upon request.

Data and code availability

The data used to support the findings of this study are available from the corresponding author upon request.

Materials

All chemicals were used as purchased without further purification. AAm, iron chloride hexahydrate ($FeCl_3 \cdot 6H_2O$), 2-propanol, 5-carboxyfluorescein, anhydrous cupric sulfate ($CuSO_4$), barium chloride ($BaCl_2$) and aluminum chloride hexahydrate ($AlCl_3 \cdot 6H_2O$) were purchased from Macklin; AA, MBAA, sodium dodecyl sulfate (SDS), tartrazine (yellow dye), 2-hydroxy-4′-(2-hydroxyethoxy)-2-methylpropiophenone, TPO, butyl acetate, sodium alginate, ammonium persulfate (APS), and *N*,*N*,*N*′,*N*′-tetramethylethylenediamine (TEMED) were purchased from Aladdin; polyvinylpyrrolidone (PVP; M_w 40,000) was purchased from Shanghai D&B Biological Science and Technology.

Preparation of photoinitiator

The preparation of the PI for stereolithography printing followed the published protocol.[27] The highly effective PI was prepared at room temperature by mixing TPO (2.6 wt %), *N*-butyl acetate (21.4 wt %), 2-propanol (21 wt %), SDS (7.5 wt %), PVP

(7.5 wt %), and DI water (40 wt %). The mixture was magnetically stirred for 1 h and freeze-dried for 3 days in a lyophilizer (FD-1A-80; Biocool). The particles were then ground into a powder and protected from light at 2°C–8°C for further use.

3D printing

The precursor for the printing of stiff fibers consists of 29 wt % AAm, 3.1 wt % AA, 4 wt % LiCl, 0.116 wt % MBAA, 0.1 wt % PI, and 0.78 μL/mL dye solution (0.1 g/mL in DI water). The precursor was mixed and degassed with a planetary mixer (Thinky ARE-300) at 2,000 rpm for 2 min before use. The solution was then loaded into a digital light printer (ENCA 3D printer). For stretch and fracture testing, specimens were printed by a setup mounted on the printer as shown in Figure S2, with a thickness of 1 mm and an exposure time of 240 s under a power of 3.51 mW/cm^2. The printed structures were sprayed with Fe^{3+} solution for ~5 s to strengthen their surfaces. The extremely soft structures can then be managed for further treatment. The printed 2D structures were washed and immersed in DI water for 24 h. To explore the factors influencing the mechanical properties of the stiff hydrogels, we changed the concentration of ferric solutions (0.02, 0.04, 0.06, and 0.08 M), the immersion time in ferric solution (0, 3, 5, 7, and 9 h), and the weight ratio of AA/AAm (7 wt %, 10.69 wt %, 14.64 wt %, and 18.89 wt %).

Heterogeneous hydrogel of 2D shapes

After immersion in DI water for 24 h, the stiff hydrogels were transferred into a mold sandwiched by two glass plates with a silicone spacer (thickness, 1.8 mm). A soft hydrogel matrix (AAm 24 wt %, MBAA 0.02 wt %. 0.01 wt % APS, and 0.15 μL/mL TEMED) was then cast on it in an argon atmosphere.

3D structures

The designed 3D structures were established in Inventor (Autodesk) and then sliced by Encashape v2.2.3 with a layer height of 50 μm. The PAAm-PAA solution was loaded into a digital light printer. The UV light power was set to be 7.14 mW/cm^2, and the printing time of each layer was set as 2.4 s.

Hydrogel heart valve

The patient vessel image was obtained by a Siemens Somatom Definition Flash dual-source computed tomography (CT) machine. The CT image was loaded into a Mimics Medical 21.0 (Materialise) and the valve parts marked and extracted. The model was then repaired by 3-Matic Medical 13.0 (Materialise) and sliced with a layer height of 50 μm for printing. The homogeneous valve was printed using PAAm-PAA precursor with each layer time of 2.4 s and UV power of 7.14 mW/cm^2. For the heterogeneous valve skeleton, the model was obtained from the Blender and then printed according to the above procedure. The printed skeleton was submerged in Fe^{3+} solution (0.04 M) for 5 h and immersed in DI water for 24 h. The skeleton was cast with a soft hydrogel matrix in a solid model to form a composite.

In vitro valve testing

The *in vitro* valve testing system consists of a pump (Suzhou Medical Implant Device, SHS-1000), a connecting tube (silicone tube with inner diameter of 16 mm and 19 mm), a manometer (Benetech GM511), an endoscope (Teslong NTS100R), and a specific gripping flange. The valve was clamped by a connector and linked onto the tube as shown in Figure S13. The water cycles when the pump works and the valve opens and closes repeatedly. The pressure drop was measured at the two sides across the valve by the manometer connected to a computer. An endoscope was used to observe the movement of the valve.

Mechanical tests

The specimens for the tensile test were cut into a dumbbell shape with 2 mm in width and 12 mm in gauge length. For the pure shear test, a rectangle of 50 mm × 30 mm was cut with a laser cutter and a crack of 10 mm was introduced in the middle plane. The tensile and pure shear tests were performed by a universal tensile machine (Smadazu AGS-X) with a loading velocity of 50 mm/min. For fatigue tests, we prepared a hybrid hydrogel with a circle (~7.3 mm in diameter) layout of stiff hydrogel and a soft hydrogel matrix. The composition of the soft hydrogel was 24 wt % AAm, 0.02 wt % MBAA, 0.01 wt % APS, and 0.15 μL/mL TEMED. The tensile speed was 5 mm/s and the $10{,}000^{th}$ cycle was set as the ending cycle due to the long time duration of the fatigue experiment. When $\lambda = 2.4$, the composite specimens broke at the clamped edge, and we took a complete specimen that can sustain 70 cycles to calculate the energy release rate.

Peeling test

The stiff hydrogel was fabricated first. The soft matrix cast on the stiff hydrogel was prepared with different concentrations of PI to form adhesion. In brief, the precursor consists of 24 wt % AAm and 0.02 wt % MBAA. We find that the gelation rate affects the adhesion properties, whereby faster gelation leads to weaker adhesion. For slow gelation, 0.01 wt % APS and 0.15 μL/mL TEMED were added. For fast gelation, 0.03 wt % APS and 0.45 μL/mL wt % TEMED were added. The peeling specimen was 15 mm in width and 100 mm in length with a precrack of 1 mm. The peeling speed was 50 mm/min by using a universal tensile machine (Smadazu AGS-X). The soft matrix layers were glued to A4 typing paper (Double-A, A4 80G) by cyanoacrylate (Loctite 406) as the backing layer. The stiff layer had no backing because it showed a much higher modulus than the soft layer.

Diffusion measurement

The stiff hydrogels were prepared first. They were then submerged in a soft hydrogel precursor with a fluorescein, 5-carboxyfluorescein (concentration, 1×10^{-4} M). The fluorescence test was performed by a confocal microscope (Nikon A1+) on the cross-section to observe the depth of the fluorescein permeated.

PAAm-alginate hydrogel

We prepared AAm-alginate precursor with AAm 12 wt %, alginate 1.8 wt %, MBAA 0.02 wt %, and PI 0.2 wt %. The PAAm-alginate hydrogel was printed with a dumbbell shape. The printed hydrogel was then submerged into various saline solutions (Fe^{3+}, Al^{3+}, Cu^{2+}, and Ba^{2+}) with a concentration of 0.1 M for 5 h and then immersed in DI water for 24 h.

Different soft matrices

We prepared several soft matrices for the composite hydrogel, namely PNIPAm, PHEMA, and gelatin. For PNIPAm, the recipe is 12 wt % NIPAm, 0.02 wt % MBAA, 0.03 wt % APS, and 0.45 μL/mL TEMED. For PHEMA, the composition is 24 wt % HEMA, 0.02 wt % MBAA, 0.03 wt % APS, and 0.45 μL/mL TEMED. The PNIPAm and PHEMA hydrogel were polymerized in an argon atmosphere. For gelatin hydrogel, 24 wt % gelatin was dissolved in DI water under 70°C and cast on the patterned stiff hydrogel. The composite was then heated for 30 min for the entanglement with the skeleton.

SUPPLEMENTAL INFORMATION

Supplemental information can be found online at https://doi.org/10.1016/j.matt.2021.03.011.

ACKNOWLEDGMENTS

This research was supported by the National Natural Science Foundation of China (nos. 11702208, 11820101001), China Postdoctoral Science Foundation (nos. BX201700192, 2018M643620), and the Harvard University Materials Research Science and Engineering Center (DMR-2011754). The authors thank Prof. Jian Yang of Xijing Hospital for providing CT image data, and Xi'an Ma Ke Medical for the flow circulation system.

AUTHOR CONTRIBUTIONS

H.Y. and M.J. contributed equally to this work. Z.S., J.T., and H.Y. designed the research. M.Y., M.S., Y.P., Y.Z., and H.J.Q. helped with the experiments. All authors contributed to the writing of the paper.

DECLARATION OF INTERESTS

The authors declare no competing interests. A patent for this fabrication strategy has been filed.

Received: December 9, 2020
Revised: February 22, 2021
Accepted: March 9, 2021
Published: March 29, 2021

REFERENCES

1. Slaughter, B.V., Khurshid, S.S., Fisher, O.Z., Khademhosseini, A., and Peppas, N.A. (2009). Hydrogels in regenerative medicine. Adv. Mater. *21*, 3307–3329.
2. Fan, H.L., and Gong, J.P. (2020). Fabrication of bioinspired hydrogels: challenges and opportunities. Macromolecules *53*, 2769–2782.
3. Bai, R., Yang, J., and Suo, Z. (2019). Fatigue of hydrogels. Eur. J. Mech. A Solids *74*, 337–370.
4. Rock, C.A., Han, L., and Doehring, T.C. (2014). Complex collagen fiber and membrane morphologies of the whole porcine aortic valve. PLoS One *9*, e86087.
5. Lee, A., Hudson, A.R., Shiwarski, D.J., Tashman, J.W., Hinton, T.J., Yerneni, S., Bliley, J.M., Campbell, P.G., and Feinberg, A.W. (2019). 3D bioprinting of collagen to rebuild components of the human heart. Science *365*, 482–487.
6. Kumar, V., Abbas, A.K., Fausto, N., and Aster, J.C. (2014). Robbins and Cotran Pathologic Basis of Disease, professional edition (Elsevier Health Sciences).
7. Hoffman, A.S. (2012). Hydrogels for biomedical applications. Adv. Drug Deliv. Rev. *64*, 18–23.
8. Moroni, L., Burdick, J.A., Highley, C., Lee, S.J., Morimoto, Y., Takeuchi, S., and Yoo, J.J. (2018). Biofabrication strategies for 3D in vitro models and regenerative medicine. Nat. Rev. Mater. *3*, 21–37.
9. Zhang, Y.S., and Khademhosseini, A. (2017). Advances in engineering hydrogels. Science *356*, eaaf3627.
10. Van Vlierberghe, S., Dubruel, P., and Schacht, E. (2011). Biopolymer-based hydrogels as scaffolds for tissue engineering applications: a review. Biomacromolecules *12*, 1387–1408.
11. Liu, X.Y., Liu, J., Lin, S.T., and Zhao, X.H. (2020). Hydrogel machines. Mater. Today *36*, 102–124.
12. Wegst, U.G., Bai, H., Saiz, E., Tomsia, A.P., and Ritchie, R.O. (2015). Bioinspired structural materials. Nat. Mater. *14*, 23–36.
13. Yang, J., Bai, R., Chen, B., and Suo, Z. (2020). Hydrogel adhesion: a supramolecular synergy of chemistry, topology, and mechanics. Adv. Funct. Mater. *30*, 1901693.
14. Yuk, H., Zhang, T., Lin, S., Parada, G.A., and Zhao, X. (2016). Tough bonding of hydrogels to diverse non-porous surfaces. Nat. Mater. *15*, 190–196.
15. Liu, Q., Nian, G., Yang, C., Qu, S., and Suo, Z. (2018). Bonding dissimilar polymer networks in various manufacturing processes. Nat. Commun. *9*, 846.
16. Wirthl, D., Pichler, R., Drack, M., Kettlguber, G., Moser, R., Gerstmayr, R., Hartmann, F., Bradt, E., Kaltseis, R., and Siket, C.M. (2017). Instant tough bonding of hydrogels for soft machines and electronics. Sci. Adv. *3*, e1700053.
17. Li, J., Celiz, A., Yang, J., Yang, Q., Wamala, I., Whyte, W., Seo, B., Vasilyev, N., Vlassak, J., and Suo, Z. (2017). Tough adhesives for diverse wet surfaces. Science *357*, 378–381.
18. Yang, J., Bai, R., and Suo, Z. (2018). Topological adhesion of wet materials. Adv. Mater. *30*, 1800671.
19. Zhao, X. (2014). Multi-scale multi-mechanism design of tough hydrogels: building dissipation into stretchy networks. Soft Matter *10*, 672–687.
20. King, D.R., Sun, T.L., Huang, Y., Kurokawa, T., Nonoyama, T., Crosby, A.J., and Gong, J.P. (2015). Extremely tough composites from fabric reinforced polyampholyte hydrogels. Mater. Horizon. *2*, 584–591.
21. Huang, Y., King, D.R., Sun, T.L., Nonoyama, T., Kurokawa, T., Nakajima, T., and Gong, J.P. (2017). Energy-dissipative matrices enable synergistic toughening in fiber reinforced soft composites. Adv. Funct. Mater. *27*, 1605350.
22. Liao, I.C., Moutos, F.T., Estes, B.T., Zhao, X., and Guilak, F. (2013). Composite three-dimensional woven scaffolds with interpenetrating network hydrogels to create functional synthetic articular cartilage. Adv. Funct. Mater. *23*, 5833–5839.
23. Wang, Z., Xiang, C., Yao, X., Le Floch, P., Mendez, J., and Suo, Z. (2019). Stretchable materials of high toughness and low hysteresis. Proc. Natl. Acad. Sci. U S A *116*, 5967–5972.
24. Li, C.H., Yang, H., Suo, Z.G., and Tang, J.D. (2020). Fatigue-Resistant elastomers. Journal of the Mechanics and Physics of Solids *134*, 103751, https://doi.org/10.1016/j.jmps.2019.103751.
25. Xiang, C., Wang, Z., Yang, C., Yao, X., Wang, Y., and Suo, Z. (2019). Stretchable and fatigue-resistant materials. Mater. Today *34*, 7–16.
26. Lake, G., and Thomas, A. (1967). The strength of highly elastic materials. Proc. R. Soc. Lond. A Math. Phys. Sci. *300*, 108–119.
27. Pawar, A.A., Saada, G., Cooperstein, I., Larush, L., Jackman, J.A., Tabaei, S.R., Cho, N.J., and Magdassi, S. (2016). High-performance 3D printing of hydrogels by water-dispersible photoinitiator nanoparticles. Sci. Adv. *2*, e1501381.

28. Zhang, B., Li, S.Y., Hingorani, H., Serjouei, A., Larush, L., Pawar, A., et al. (2018). Highly stretchable hydrogels for UV curing based high-resolution multimaterial 3D printing. Journal of Materials Chemistry B *6*, 3246–3253, https://doi.org/10.1039/c8tb00673c.

29. Grigoryan, B., Paulsen, S.J., Corbett, D.C., Sazer, D.W., Fortin, C.L., Zaita, A.J., Greenfield, P.T., Calafat, N.J., Gounley, J.P., Ta, A.H., et al. (2019). Multivascular networks and functional intravascular topologies within biocompatible hydrogels. Science *364*, 458–464.

30. Lin, P., Ma, S., Wang, X., and Zhou, F. (2015). Molecularly engineered dual-crosslinked hydrogel with ultrahigh mechanical strength, toughness, and good self-recovery. Adv. Mater. *27*, 2054–2059.

31. Zheng, S.Y., Shen, Y., Zhu, F., Yin, J., Qian, J., Fu, J., Wu, Z.L., and Zheng, Q. (2018). Programmed deformations of 3D-printed tough physical hydrogels with high response speed and large output force. Adv. Funct. Mater. *28*, 1803366.

32. Truby, R.L., and Lewis, J.A. (2016). Printing soft matter in three dimensions. Nature *540*, 371–378.

33. Deng, S.H., Wu, J.J., Dickey, M.D., Zhao, Q., and Xie, T. (2019). Rapid open-air digital light 3D printing of thermoplastic polymer. Adv. Mater. *31*, 1903970.

34. Yang, C.H., Wang, M.X., Haider, H., Yang, J.H., Sun, J.Y., Chen, Y.M., Zhou, J.X., and Suo, Z.G. (2013). Strengthening alginate/polyacrylamide hydrogels using various multivalent cations. ACS Appl. Mater. Interfaces *5*, 10418–10422.

35. Yang, C.H., and Suo, Z.G. (2018). Hydrogel ionotronics. Nat. Rev. Mater. *3*, 125–142.

36. Thomas, A.G. (1958). Rupture of rubber. 5. Cut growth in natural rubber vulcanizates. J. Polym. Sci. *31*, 467–480.

37. Lin, S., Liu, X., Liu, J., Yuk, H., Loh, H.-C., Parada, G.A., Settens, C., Song, J., Masic, A., and McKinley, G.H. (2019b). Anti-fatigue-fracture hydrogels. Sci. Adv. *5*, eaau8528.

38. Taylor, D., O'Mara, N., Ryan, E., Takaza, M., and Simms, C. (2012). The fracture toughness of soft tissues. J. Mech. Behav. Biomed. Mater. *6*, 139–147.

39. Mirnajafi, A., Zubiate, B., and Sacks, M.S. (2010). Effects of cyclic flexural fatigue on porcine bioprosthetic heart valve heterograft biomaterials. J. Biomed. Mater. Res. A *94*, 205–213.

40. Gong, J.P., Katsuyama, Y., Kurokawa, T., and Osada, Y. (2003). Double-network hydrogels with extremely high mechanical strength. Adv. Mater. *15*, 1155–1158.

41. Hu, J., Hiwatashi, K., Kurokawa, T., Liang, S.M., Wu, Z.L., and Gong, J.P. (2011). Microgel-reinforced hydrogel films with high mechanical strength and their visible mesoscale fracture structure. Macromolecules *44*, 7775–7781.

42. Lin, S., Liu, J., Liu, X., and Zhao, X. (2019a). Muscle-like fatigue-resistant hydrogels by mechanical training. Proc. Natl. Acad. Sci. U S A *116*, 10244–10249.

43. Zhang, W., Hu, J., Tang, J., Wang, Z., Wang, J., Lu, T., and Suo, Z. (2018). Fracture toughness and fatigue threshold of tough hydrogels. ACS Macro Lett. *8*, 17–23.

44. Kuang, X., Roach, D.J., Wu, J.T., Hamel, C.M., Ding, Z., Wang, T.J., Dunn, M.L., and Qi, H.J. (2019). Advances in 4D printing: materials and applications. Adv. Funct. Mater. *29*, 1805290.

45. Oveissi, F., Naficy, S., Lee, A., Winlaw, D., and Dehghani, F. (2020). Materials and manufacturing perspectives in engineering heart valves: a review. Mater. Today Biol. *5*, 100038.

46. Sacks, M.S., Merryman, W.D., and Schmidt, D.E. (2009). On the biomechanics of heart valve function. J. Biomech. *42*, 1804–1824.

47. Zheng, S.Y., Ding, H., Qian, J., Yin, J., Wu, Z.L., Song, Y., and Zheng, Q. (2016). Metal-coordination complexes mediated physical hydrogels with high toughness, stick–slip tearing behavior, and good processability. Macromolecules *49*, 9637–9646.